Ion jet properties in a high current – short duration vacuum arc thruster with and without magnetic field

IEPC-2022-508

Presented at the 37th International Electric Propulsion Conference
Massachusetts Institute of Technology, Cambridge, MA USA
June 19-23, 2022

T.Yung*, A.Blanchet† and L.Herrero‡
Comat[1], Toulouse, 31130, France

The Plasma Jet Pack (PJP) is a vacuum arc thruster (VAT) developed from scratch by Comat since 2015. This technology, based on the vacuum arc physics, takes advantage of using solid metal propellant. It offers a high specific impulse (> 2500s) combined to a global thrust-to-power higher than 6µN/W, and this, in a small volume (~1U) without any pre-heating process or safety integration constraints. The specificity of this VAT is the arc discharge characteristics, defined by a short duration (10-30µs) length and a high arc current (2-5kA). This paper focuses on the effects of the magnetic field on several parameters, including the mean ion charge and velocity of the plasma flow, which are calculated by an indirect way. Indeed, these parameters are determined thanks to three measurements: the propellant mass eroded per pulse, the ion current as a function of time, of angle and of impulse bit.

I. Nomenclature

C_X	=	Focalization ratio
e	=	Elementary charge
f	=	Operating frequency
g_0	=	Standard acceleration due to gravity
I	=	Ion current
I_{bit}	=	Impulse bit
I_{sp}	=	Specific impulse
m_i	=	Ion mass
$m_{p/pulse}$	=	Propellant mass eroded per pulse
$\dot{n_{is}}$	=	Ion flow emitted at the cathode
$\dot{n_i}$	=	Ion flow received on the probe
q	=	Charge
R	=	Distance between the cathode surface and the Langmuir probe
S	=	Probe area
T	=	Thrust
$\overline{v_i}$	=	Mean ion velocity
Z	=	Mean charge state

* PJP Technical Manager, Comat innovation department, t.yung@comat.space
† PJP Product Manager, Comat innovation department, a.blanchet@comat.space
‡ BU Product Officer, Comat innovation department, l.herrero@comat.space

II. Introduction

COMAT[1] has been designing, manufacturing, qualifying and commercializing equipment for the space industry since 1977. Located in Toulouse, in the heart of a unique technological ecosystem, COMAT has been providing instruments and flight equipment for years. From understanding client needs to exploiting products, COMAT has a solid team of highly qualified experts. With its unique industrial capacity, COMAT design office has evolved over the years to become the digital factory of tomorrow. COMAT, a space pure player, puts its 45 years of existence and expertise to the service of its clients.

In the "small sat" business unit of the company, the Plasma Jet Pack (PJP) is the most innovative technology developed from scratch. Since 2015, the R&D COMAT teams have been working in collaboration with European laboratories to build the most efficient vacuum arc thruster module.

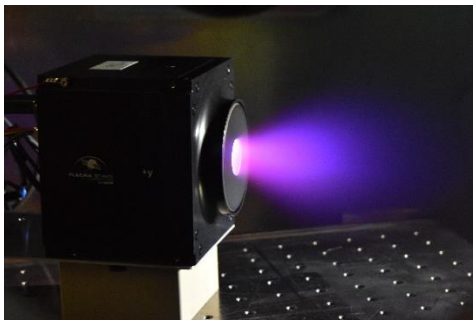

Figure 1. PJP firing in COMAT facilities.

The vacuum arc thruster (VAT) physics allows eroding solid metal propellant thanks to electrical discharge in vacuum. After an ignition process, an electric breakdown takes place between cathode and anode electrodes. During the arc, craters named "cathode spot" appear on the cathode surface; these spots result from heating process (Joule effect and ion bombardment) in the cathode sheath. The plasma jet is characterized by high currents (2-5kA) and short pulses duration (10 - 30µs).

The cathode is ablated and solid metal is first transformed into vapor then into plasma by an electronic avalanche mechanism in the ionization region. Then, the plasma is accelerated thanks to electromagnetic mechanism and ejected from the thruster. For few Joules energy discharge, the order of magnitude of ion exhaust velocity is higher than 20km/s (depending on the cathode material) and the mass eroded per pulse is about the micrograms. These benefits, such as solid metal propellant and high specific impulse (>2000s), allow this electric propulsion technology to target the small satellite market.

Figure 2. PJP Flight Model for ISIS Space IOD/IOV mission.

The vacuum arc has been extensively studied by Boxman et al. among others[2,3], and has applications in metallic coating deposition, ion source, high current interrupters, etc.

However, in spite of extensive scientific research on the vacuum arc physics, VAT suffers from a lack of experimental feedbacks and theoretical studies to better understand the physics phenomena, especially the ion acceleration mechanism. Testing requires specific probes and diagnostics in order to withstand the noisy VAT electromagnetic environment for such a high current/short duration system.

The purpose of this study is to indirectly measure the ion mean charge and the ion velocity by using three combined measurements: thrust, erosion rate, and cone angle. This experimental study has been performed with the same PJP model for titanium and brass cathode with and without magnetic nozzle.

Having reminded the equations giving the mean charge and the mean ion velocity, we will detail our experimental campaign and facilities for each step. Then, we will expose the results with an error analysis and discuss about the cathode material and magnetic nozzle impacts on the plume.

III. Experimental campaign description

A. Indirect measurement of Z and $\bar{v}_i$ – equations set

The mean ion charge Z and the mean ion velocity $\bar{v}_i$ can be calculated indirectly by using 3 complementary measurements:

- The propellant mass eroded per pulse $m_{p/pulse}$
- The ion current emitted as a function of time and angle $I(\theta, t)$
- The impulse bit (thrust on the exhaust axis) I_{bit}

With S the Langmuir probe area given in the ion saturation regime, the ion flow (at.m^{-2}s^{-1}) received by the probe can be written as:

$$\dot{n}_{is}(\theta, t) = \frac{I(\theta, t)}{eZS} \tag{1}$$

By using a Langmuir probe at a distance R from the cathode emission plane, the ion flux (at.s^{-1}) emitted at the cathode is given by integrating the previous equation over an hemisphere:

$$\dot{n}_{is}(\theta, t) = \frac{I(\theta, t)}{eZS} \tag{1}$$

$$\dot{n}_i(t) = \int_{\theta=0}^{\frac{\pi}{2}} \int_{\varphi=0}^{2\pi} \dot{n}_{is}(\theta, t) \cdot R^2 \, sin(\theta) \, d\theta d\varphi \tag{2}$$

With m_i the atomic mass of the ion, the previous equations can be used to define the mass eroded per pulse:

$$m_{p/pulse} = m_i \cdot \int_0^{t_p} \dot{n}_i(t) dt \tag{3}$$

The focalization ratio on the exhaust axis X can be written as follows:

$$C_X = \frac{\int_{\theta=0}^{\frac{\pi}{2}} I(\theta, t) \cdot \cos\theta \sin\theta \, d\theta}{\int_{\theta=0}^{\frac{\pi}{2}} I(\theta, t) \cdot \sin\theta \, d\theta} \tag{4}$$

Then, the global thrust and the thrust component on the exhaust axis X can be written as:

$$|\boldsymbol{T}(\boldsymbol{t})| = m_i v_i \dot{n}_i(t) \tag{5}$$

$$T_X(t) = C_X \cdot |\boldsymbol{T}(\boldsymbol{t})| \tag{6}$$

Finally, the measured impulse bit is given with the following equation:

$$I_{bit} = \int_0^{t_p} T_X(t) dt \tag{7}$$

By gathering the defined equations, the unknowns Z and $\bar{v}_i$ can be calculated by solving numerically the following set of equations:

$$Z = \frac{m_i 2\pi R^2}{m_{p/pulse} eS} \cdot \int_0^{t_p} \int_{\theta=0}^{\frac{\pi}{2}} I(\theta, t) \cdot \cos(\theta) \, d\theta \, dt \tag{8}$$

$$\bar{v}_i = \frac{I_{bit}}{C_X \cdot m_{p/pulse}} \tag{9}$$

B. Flow chart

The aim of the study is to determine the mean charge and the mean velocity of the exhausted ions. Consequently, the three necessary parameters described in the previous section $\left(m_{p/pulse}, I_{bit}\right.$ and $\left.I(\theta,t)\right)$ are measured as follows.

To obtain the mass eroded per pulse, the mass of the cathode is measured before assembly of the thruster on a precision balance (resolution: 0.001g) and after a sequence of N pulses. The mass eroded per pulse is then given by the mass difference divided by the number of pulses.

Then the impulse bit is given by measuring the thrust while the PJP is operating at a constant frequency. Then the impulse bit is given by calculating the thrust divided by the frequency.

Finally, the ion current is measured with a Langmuir probe set to a potential of -60V, in the ion saturation regime, for angles from 0° to 90°.

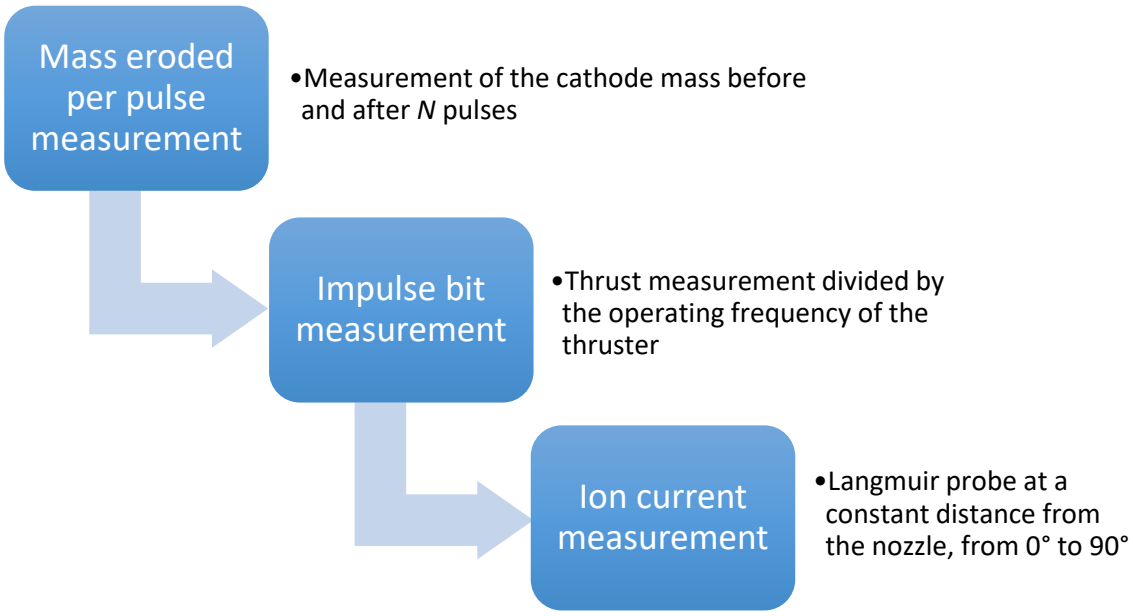

Figure 3. Measurement process flow chart.

C. COMAT Facilities

Comat propulsion laboratory is set in an ISO8 clean room. In this clean room, a 0.5m^3 vacuum chamber allows to have a space representative vacuum environment of 10^{-6} mbar. The propulsion setup is composed of one thrust bench, several homemade Langmuir probes, a 2D translation table and 4 channels Rode & Schwartz RTE 1024 high speed oscilloscope (200MHz bandwidth, 5 Gsample/s per channel).

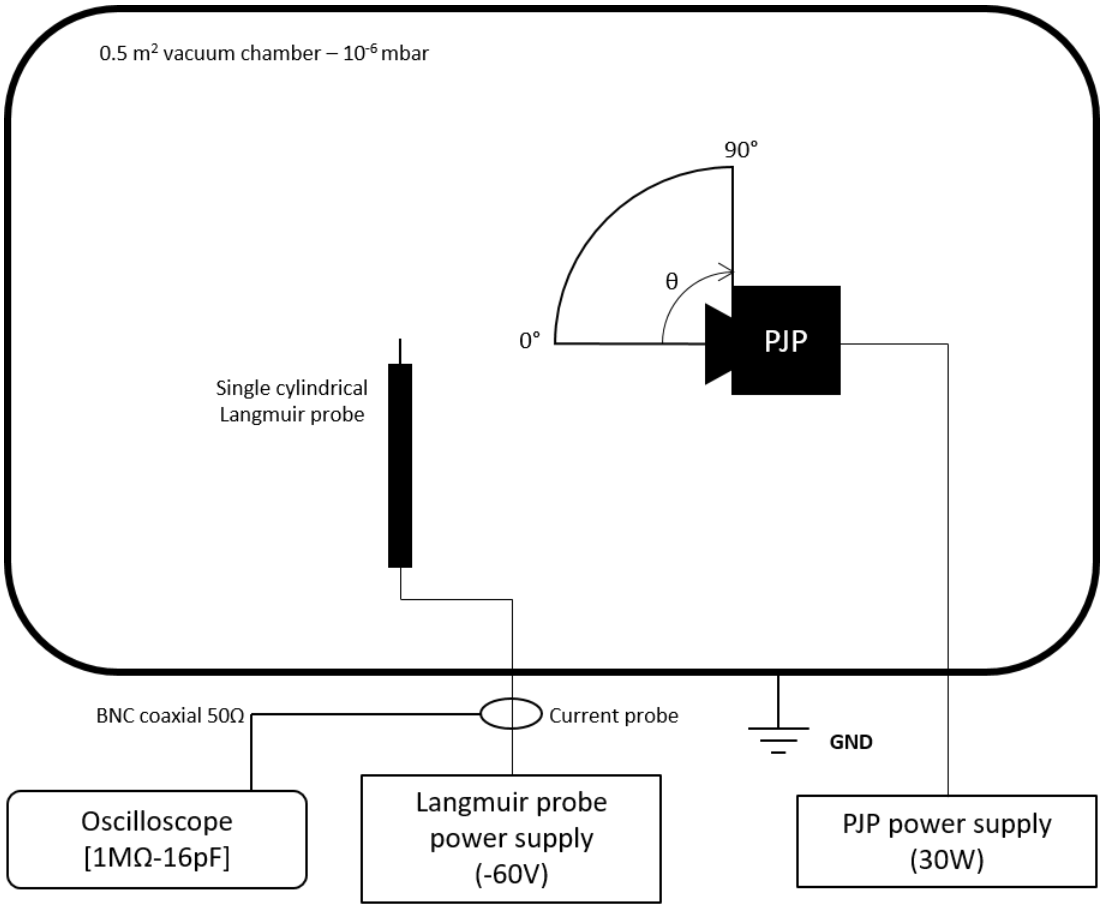

Figure 4. Diagram of the experimental facility

D. Thrust measurement description

Since 2017, COMAT has been using its own test facilities to measure the Plasma Jet Pack performances. Thrust measurement is carried out by internal homemade torsional pendulum with the following capabilities:

Sensitivity	7.63	µm/µN
Max load	5.8	kg
Max thrust measurable	620	µN
Resolution	0.19	µN

Table 1. COMAT Thrust bench capabilities

COMAT successfully qualified this thrust bench thanks to the CNES agency and the ONERA Palaiseau Laboratory in 2019 for the following measurements[4]:

- **"Mean thrust" Method** – Measure of the mean thrust by setting the thruster at a constant operating frequency or continuous.
- **"Impulse" Method** – Measure of the impulse bit for each plasma pulse (only for pulsed thruster)

The principle is as follows: the operating thruster is aligned in front of a target (mica screen). The exhausted plasma pushes the target and moves a pendulum arm around its axis of rotation (z). On the other side of the arm, the oscillatory motion of the pendulum is raised thanks to a capacitive sensor. The rotation axis is physically represented by a torsional wire mounted on a chuck.

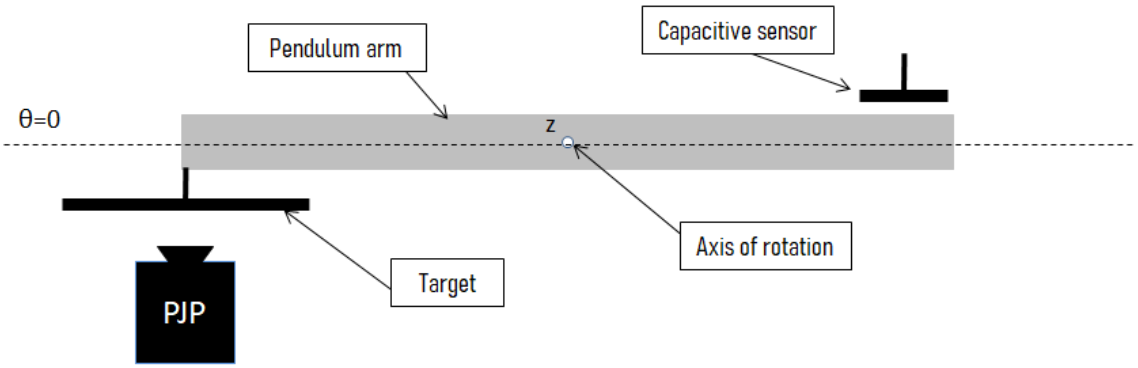

Figure 5. COMAT Torsional thrust bench description.

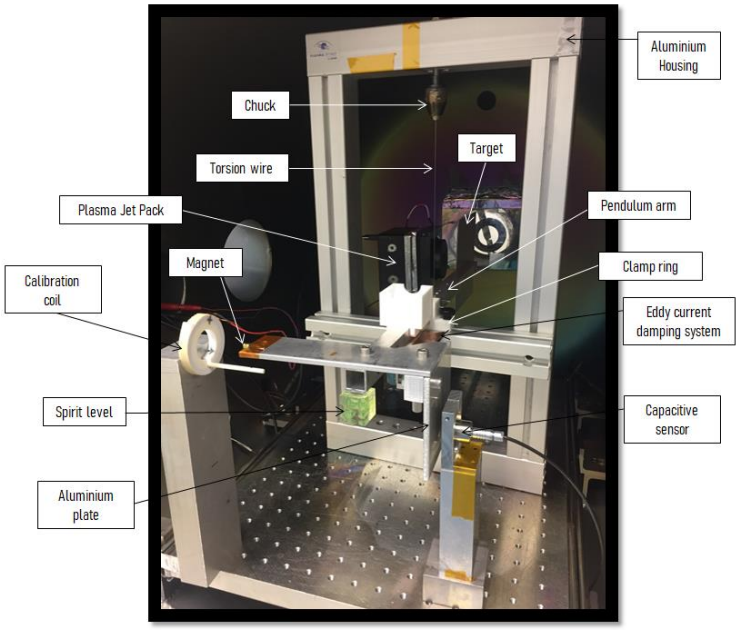

Figure 6. COMAT torsional pendulum description.

The thrust measurement is composed of 3 steps:

1. Torsional pendulum calibration
2. Force coil calibration
3. Thrust measurement under vacuum

E. Cone angle measurement description

The focus of the plasma flow is described by a measurement named the cone angle. It represents the conical region where 95% of the plasma jet is present. It was decided to consider the ion charge instead of the ion density. Indeed, the total ion charge emitted by the thruster depends on two parameters: the number of ions and the charge of each one of them.

To find the total ion charge, the ion current was measured by a Langmuir probe which was put at a constant distance from the center of the cathode and was set to a potential of -60V. This electric potential allows to screen the electrons and to only catch the ions. Measurements were performed every 10° from 0° to 90°. This angle corresponds to the angle between the thrust direction and the probe. Since each pulse is not identical to the others, a statistical study was realized by performing a hundred of measurements for each angle. Once the ion current is measured on the oscilloscope, the charge q is calculated by realizing the trapezoidal numerical integration of the current I:

$$q = \int_0^{t_p} I dt \tag{10}$$

With t_p, the time length of the pulse. The mean charge values for each angle form a curve and the cone angle is the angle α_{95} for which the area under the curve represents 95% of the total area:

$$\frac{\int_{0°}^{\alpha_{95}} q d\varphi}{\int_{0°}^{90°} q d\varphi} = 0{,}95 \tag{11}$$

With $d\varphi$, the angle variation.

F. Specific impulse measurement description

The specific impulse is proportional to the impulse bit I_{bit}, that was previously defined, and inversely proportional to the mass eroded per pulse, which is the mass eroded per pulse, and the standard acceleration due to gravity g_0.

$$I_{sp} = \frac{I_{bit}}{m_{p/pulse} \cdot g_0} \tag{12}$$

In order to calculate the specific impulse, we firstly need to measure the thrust as previously described. Indeed, the impulse bit is equal to the thrust T divided by the frequency of the pulses during the thrust measurement f:

$$I_{bit} = \frac{T}{f} \tag{13}$$

The other value we need is the erosion rate. To calculate this value, we measured the mass of the cathode before and after several thousand pulses (>10k). The mass difference Δm (which corresponds to the mass consumption), divided by the number of pulses N, gives the erosion rate:

$$m_{p/pulse} = \frac{\Delta m}{N} \tag{14}$$

The specific impulse is also directly linked to the mean ion velocity on the exhaust axis X by the following equation:

$$\overline{v_{i,X}} = I_{sp} \cdot g_0 \tag{15}$$

IV. Results

The aim of this study is to analyze the influence of the magnetic field on the ion jet properties of the PJP. In addition, these effects are compared for two cathode materials: titanium and brass.

A. Magnetic nozzles

Consequently, it was decided to use different permanent magnets in order to create a magnetic nozzle. Three different magnets were used. The first and the second ones are radially magnetized, it means that the South Pole and the North Pole are respectively situated at the center and the periphery of the annular magnet.

The only difference between these two radially magnetized magnets is the remanence, which is equal to 0.49T for the first one and to 1.1T for the second one.

Figure 7. Radial magnet used for the magnetic nozzle

The following figures show the cartography of the magnetic lines (Figure 8). The magnetization of the magnet allows to have a zero magnetic flux density at the center of the magnet.

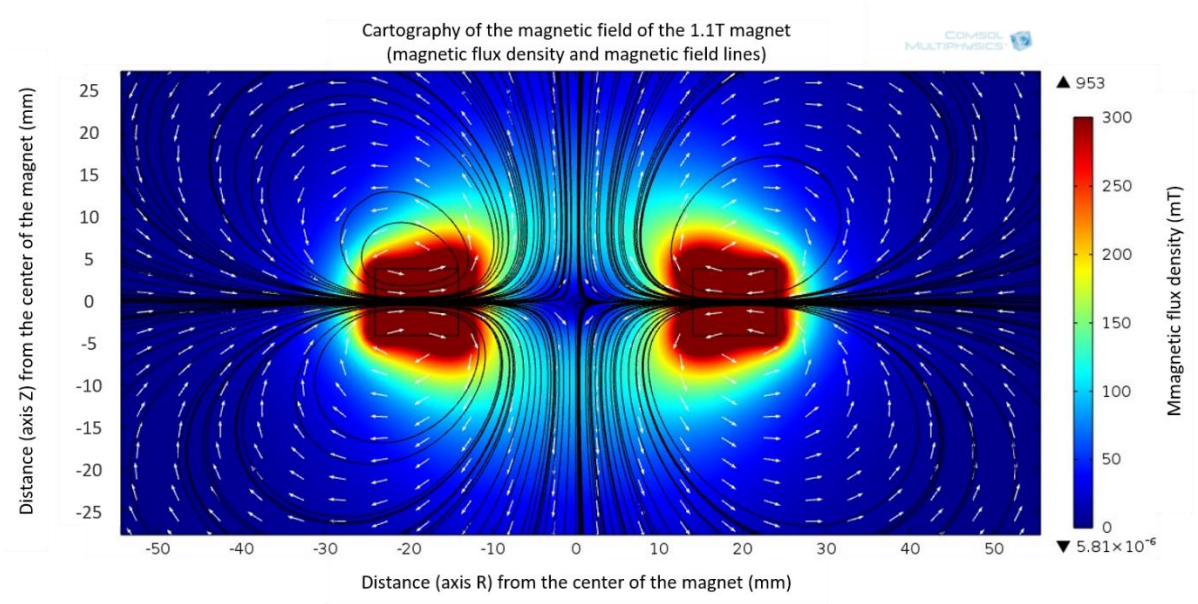

Figure 8. Cartography of the magnetic field lines of the radial magnet (1.1T magnet)

Figure 9 and Figure 10 plot the magnetic flux density along the axis of thrust (axis Z) respectively for the 1.1T radial magnet and the 0.49T magnet.

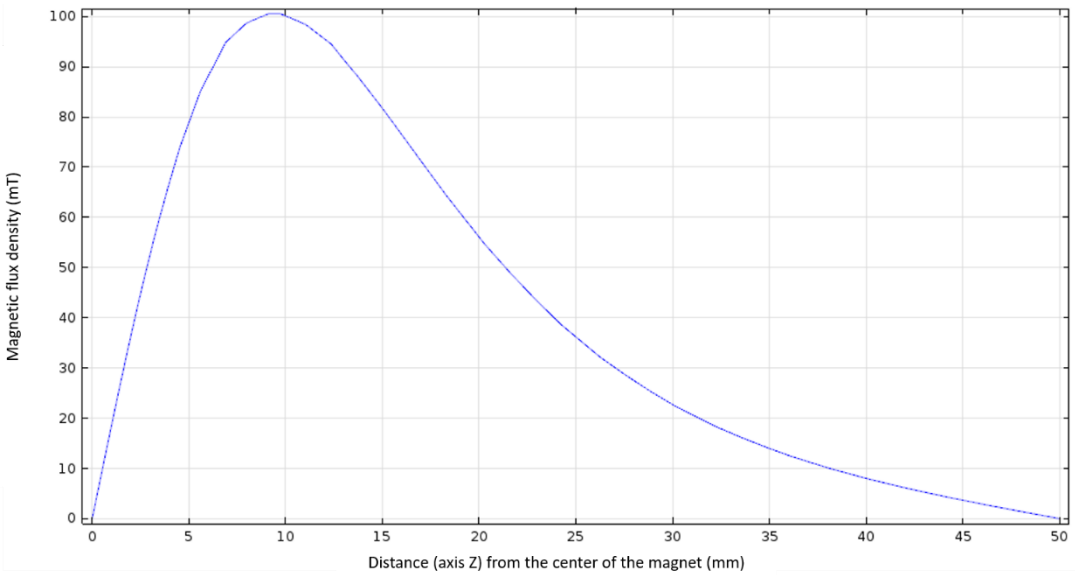

Figure 9. Magnitude of the magnetic field along the axis of thrust (1.1T magnet)

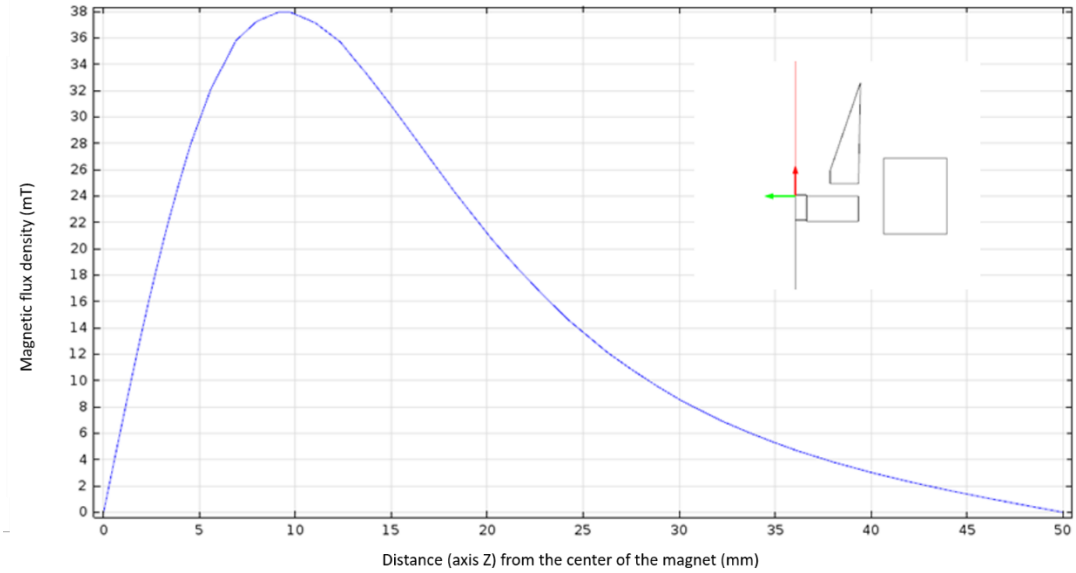

Figure 10. Magnitude of the magnetic field along the axis of thrust (0.49T magnet)

This magnetic configuration allows to have a minimal magnetic field at the center of the thruster, where the triggering arc discharge occurs. On the axis of thrust, the magnitude of the magnetic field increases, before reaching a peak at 9 mm from the center of the magnet. At this point, the magnetic field lines change their direction and the magnetic flux density drops. Upstream, the lines are converging, which tends to constrict the plasma, and then, the lines diverge. The peak of the magnitude of the magnetic field is equal to 38mT for the 0.49T magnet and 100mT for the 1.1T.

The third magnet is axially magnetized; the North Pole is on one side of the magnet and the South on the opposite side. The remanence of this last one is equal to 1.32T.

B. Uncertainty for the impulse bit and specific impulse

In this study, the relative standard uncertainty is calculated by the sum of squares of the different uncertainty sources (worst case).

The impulse bit measurement relative uncertainty, s_{TM}, comes from different sources, which are detailed in the following table:

Standard deviation s_X	**Origin**	**Value of s_X**	**Relative standard uncertainty $\frac{s_X}{X}$**
s_S	Sensor linearity	0.5 µm	0.5/Δx
s_B	Balance output – voltage noise	0.73 µm	0.73/Δx
s_k	Calibration	TBD	~ 2.6e-2
s_R	Moment arm	2 mm	1e-2
s_ς	Damping factor	~ 0	1e-4

Table 2. Impulse bit measurement uncertainties

The combined standard uncertainty, s_{TM}, is then calculated as:

$$s_{TM} = \sqrt{s_S^2 + s_B^2 + s_s^2 + s_R^2 + s_\varsigma^2} \tag{16}$$

For the specific impulse, another parameter has to be taken into account in order to calculate the uncertainty on the specific impulse. Indeed, this parameter is the uncertainty related to the measurement of the mass eroded during the pulse sequence, which is noted $s_{\Delta m}$. This mass is measured on a precision balance of a resolution of 0.001g. The uncertainty on the specific impulse is then given by:

$$s_{I_{sp}} = \sqrt{s_{TM}^2 + s_{\Delta m}^2} \tag{17}$$

C. Impulse bit results

The results of the impulse bit with the brass cathode and the titanium cathode, for the radial magnets, are presented below, in Figure 11. The impulse bit for the brass cathode is plotted in orange and the one for the titanium is plotted in grey. On the horizontal axis, the three values correspond to the remanence of the magnet in the different magnetic configurations (0T is the non-magnetic configuration). The horizontal axis represents the impulse bit in µNs. The error bars correspond to the uncertainty, as defined in section IV.B, with equation:

$$s_{TM} = \sqrt{s_S^2 + s_B^2 + s_s^2 + s_R^2 + s_\varsigma^2} \tag{16}$$

.

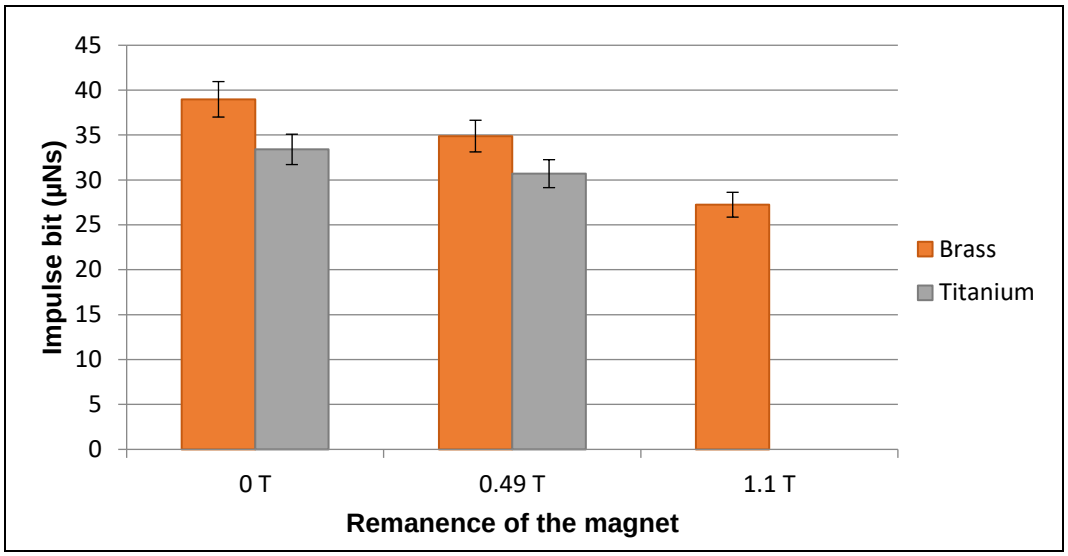

Figure 11. Impulse bit for different radially magnetized magnets (error bars represent the uncertainty)

Several impulse bit measurements were realized. The mean value is embraced by error bars which correspond to the uncertainty and are plotted in black.

The first notable thing is that the impulse bit decreases as the remanence of the radial magnet increases. This effect is visible both for brass and titanium. Between 0T and 0.49T, the drop represents about 10% of the initial impulse bit as for brass and titanium. It is more significant between 0.49T and 1.1T for brass, as the decrease of impulse bit corresponds to more than 20%.

Moreover, there is no value for titanium with the 1.1T magnet. The reason is that the initiation rate was too low with this magnet (<50%). The lack of initiation can be explained by the fact that the titanium particles eroded by the trigger arc discharge are trapped by the magnetic field and do not fill the interelectrode gap, thus not permitting the electric continuity between the anode and the cathode.

Below, in Figure 12, are presented the impulse bit measurement results for the axial magnet. The mean value is embraced by error bars which correspond again to impulse bit measurement uncertainty.

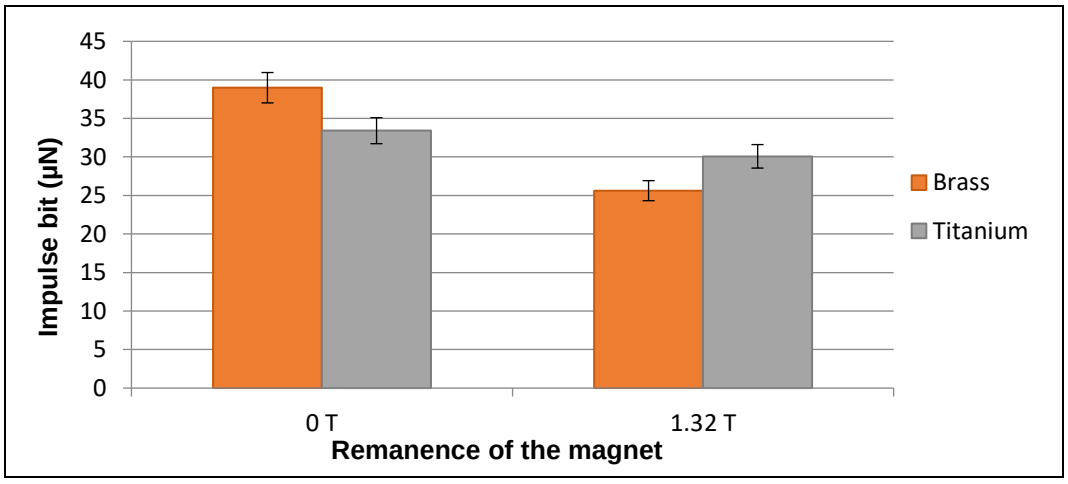

Figure 12. Impulse bit for the axially magnetized magnet (error bars represent the uncertainty)

As with the radial magnet, the remanence of the axial magnet tends to reduce the impulse bit. It is more significant with the brass cathode. Actually, the impulse bit drops from 39µNs to 26µNs with the magnet, which corresponds to a decrease of 34% of the initial value. The effects are less distinct with the titanium cathode, where the decrease only represents 10%.

D. Mass eroded per pulse

The cathode mass was measured before and after every pulse sequence. A sequence is composed of at least 10,000 pulses, in order to have a significant erosion of cathode. The following table presents the mass eroded per pulse for each cathode material and each magnetic configuration.

Cathode material / Magnet remanence	Brass	Titanium
0T	1.65 µg	1.33 µg
0.49T (radial)	1.35 µg	1.17 µg
1.1T (radial)	1.1 µg	N/A
1.32T (axial)	1.32 µg	1.14 µg

Table 3. Cathode mass eroded per pulse as function of the magnetic configuration and the cathode material

The magnetic field tends to reduce the cathode consumption whether the magnetization of the magnet is axial or radial.

E. Specific impulse

The impulse bit results are then used in order to calculate the specific impulse of the thruster. As previously mentioned, the erosion rate is measured by weighing the cathode before and after a determined number of pulses. Then, according to Eq. (12), it is possible to determine the specific impulse for each magnetic configuration, for both cathode materials.

For the radial magnets, the specific impulse is plotted in Figure 13. The specific impulse tends to increase between 0T and 0.49T and then decreases at 1.1T for brass. Nonetheless, the uncertainty is too important to conclude to a significant influence of the magnetic field on the specific impulse. Indeed, the values are all close to 2500s. The uncertainty, materialized by the error bars, is determined as described in section IV.B.

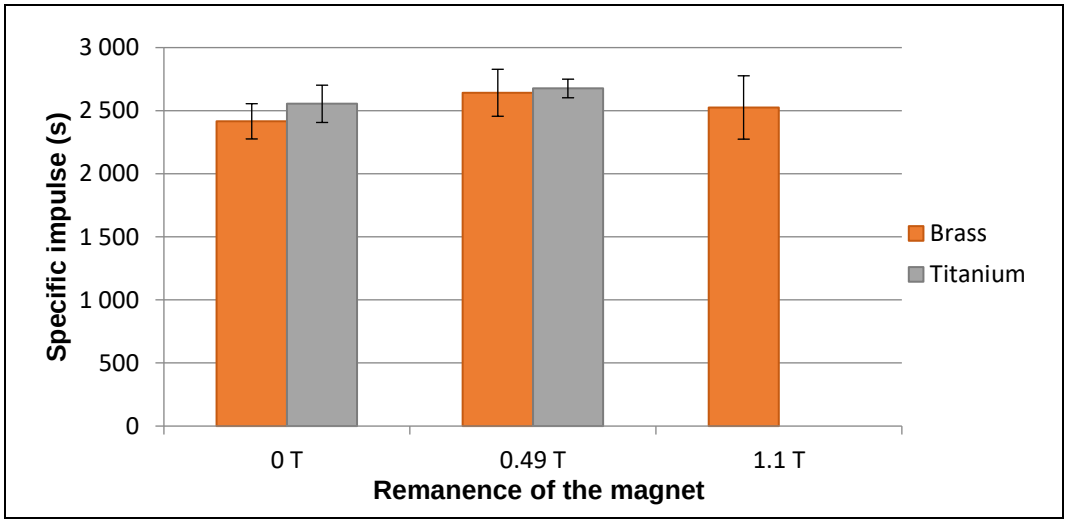

Figure 13. Specific impulse for the radially magnetized magnet (error bars represent the uncertainty)

The results for the axially magnetized magnet, which are represented in Figure 14, are quite different from the previous ones. In fact, between 0T and 1.32T of remanence, the specific impulse decreases for the brass cathode but remains almost constant for titanium. For brass, the decrease represents nearly 20% of the initial specific impulse.

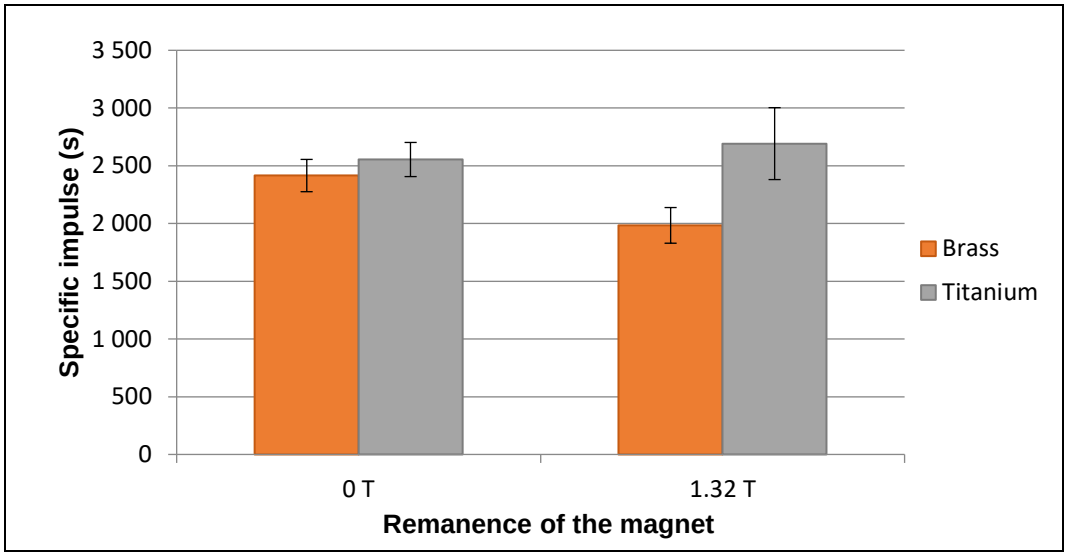

Figure 14. Specific impulse for the axially magnetized magnet (error bars represent the uncertainty)

F. Cone angle

As previously mentioned, the cone angle is described as the cone where 95% of the total charge of the plasma is contained. The point of this measurement is to have a visualization of the focus of the plasma plume. This focus is relevant for the study of the thruster because it shows the possible interactions between the plasma and other components on the satellite. Moreover, the cone angle helps to determine if the energy of the particles is well projected on the axis of thrust. Once again, the results are shown separately for the two magnetic configurations (axial and radial magnets) and for both cathode materials (brass and titanium).

The principle of this measurement is presented in section III.E. For each angle and each magnetic configuration, around 100 or 200 measurements were done. Therefore, a statistical study of the results was performed and the error bars, in the figures below, represent the 95% confidence interval, of all the n measurements, around the mean value:

$$I_{95\%} = \mu \pm \frac{2\sigma}{\sqrt{n}} \tag{18}$$

1. Radially magnetized magnets

Figure 15 and Figure 16 show the charge received on the Langmuir probe as a function of the angle for the radial magnets, respectively for the brass cathode and the titanium cathode.

For the brass cathode, the initial cone angle (without magnetic field) is equal to 62°. The graph shows that the cone angle decreases when the magnetic remanence of the magnet increases. With the 0.49T magnet, the cone angle drops to 58° and with the 1.1T magnet, it drops to 50°. The conclusion is that the magnetic field tends to focus the plasma flow. Indeed, the total charge at the periphery of the plume becomes negligeable.

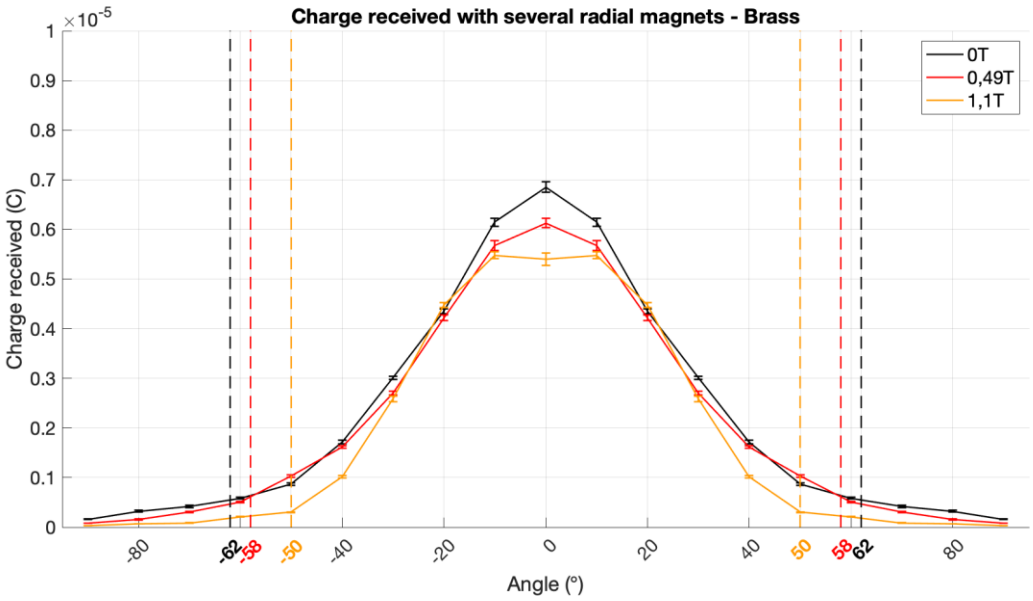

Figure 15. Cone angle for the brass cathode with different radial magnets (error bars represent the 95% confidence interval of all the *n* measurements)

Concerning the titanium cathode, the cone angle is slightly smaller, as shown in Figure 16. Without the magnetic field, the cone angle is equal to 57° instead of 62° for brass. With the 0.49T magnet, the value of the cone angle decreases to 52°.

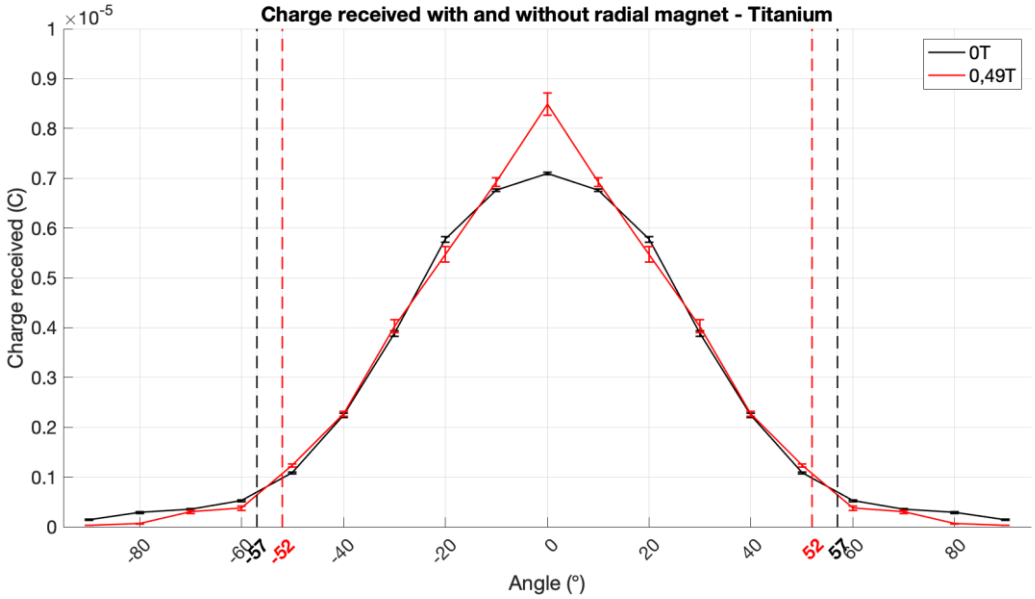

Figure 16. Cone angle for the titanium cathode with and without the radial magnet (error bars represent the 95% confidence interval of all the *n* measurements)

Even if the curves, on Figure 16, of the charge received as a function of the angle seem to be similar, the current received with and without the magnetic field has a different dynamic. Figure 17 shows the mean current received on the probe for each angle as a function of time, without magnetic field. Figure 18 presents the same data with the 0.49T radial magnet.

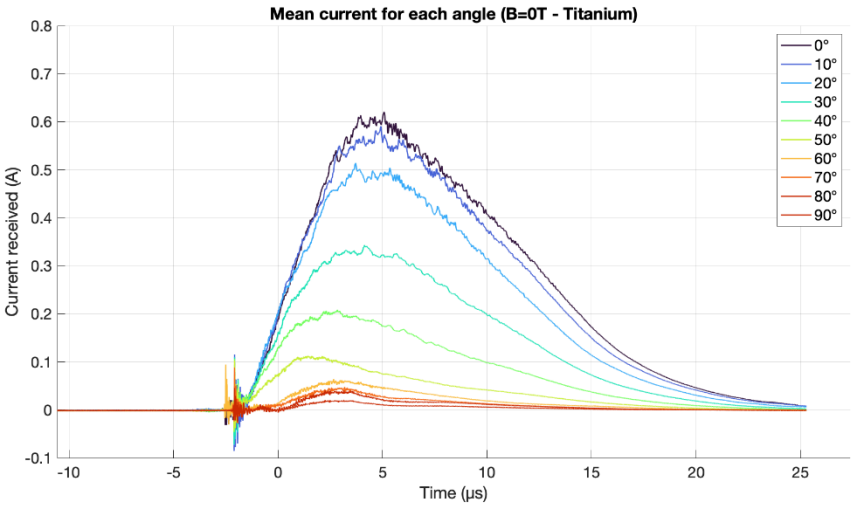

Figure 17. Mean current received on the Langmuir probe on several angles for the titanium cathode without applied magnetic field

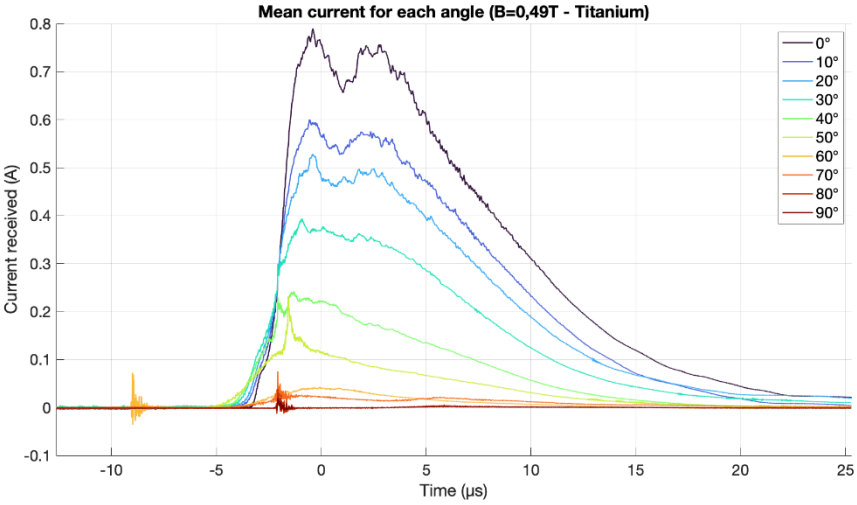

Figure 18. Mean current received on the Langmuir probe on several angles for the titanium cathode with the 0.49T radial magnet.

The main information that can be derived is that the mean current with the magnetic field has two peaks, while the one without magnetic field only has one peak. Moreover, the rising edge with the magnetic field is slightly shorter than in the non-magnetic configuration and the decrease after the peaks is also more significant with the magnet. Finally, the maximum current reached is higher with the magnetic field. The current received with the magnetic configuration is higher but with a shorter duration, consequently, as seen previously in Figure 16, the area under the curve is similar in both cases.

These observations lead to focus on the dynamic of the thrust. Impulse bit results presented in section IV.C only give a static vision of the thrust produced by one pulse. Nevertheless, it is possible to calculate the thrust as a function of time by using equations (5) and (6). The following plots give a dynamic view of the thrust during one single pulse.

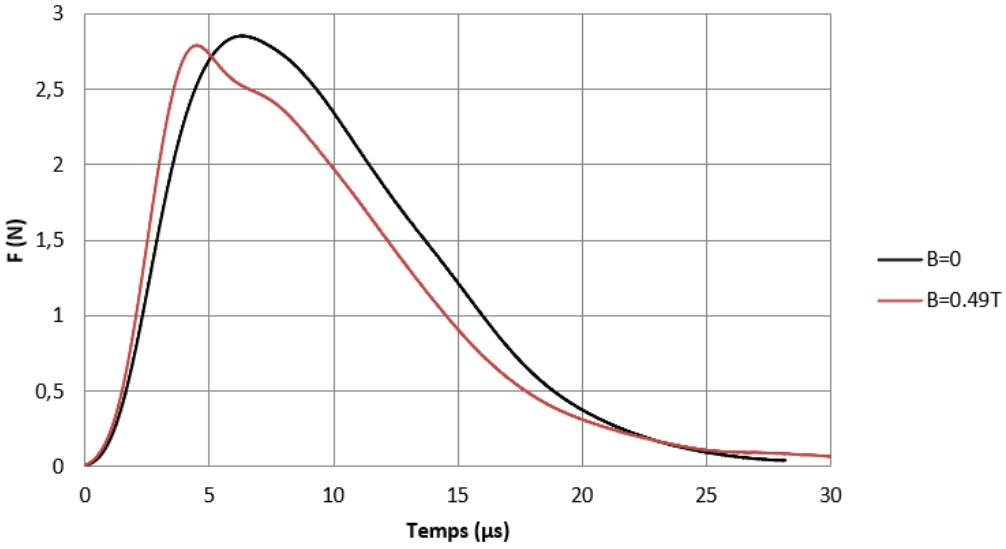

Figure 19. Thrust on the exhaust axis as function of time for the titanium cathode with and without magnetic field.

As the mean current received on the probe, the dynamic of the thrust is modified by the magnetic field. With the radial magnet, the thrust increases faster but lasts a shorter time. In addition, both configurations reach an instant thrust of 2.8N. The impulse bit actually represents the integral of these curves.

The radial magnets constrict the plasma plume without changing the global repartition of the charge. Indeed, the charge distribution is quasi-gaussian, with a maximum value at the center of the plume and a decrease along the angle, with and without the magnetic field. The drop of the cone angle value is explained by a reduction of the charge received for high angles. It means that the magnetic field acts on particles with a high exhaust angle and tends to refocus them. This magnetic configuration also focuses particles which are ejected in a direction close to the axis of thrust because the quasi-gaussian distribution is conserved.

2. Axially magnetized magnet

The results obtained with the axial magnet for the brass cathode are presented in Figure 20. Cone angle for the brass cathode with and without the axial magnet. Even if the value of the cone angle is almost the same, the spatial repartition of the charges is not similar. The previous measurements and the non-magnetic configuration showed a quasi-gaussian distribution of the charges as a function of the angle. Conversely, with the 1.32T axial magnet, the charge received by the Langmuir probe between 0° and 30° is almost constant. For the higher angles, the values are similar to the non-magnetic configuration.

Moreover, as previously, the total charge exhausted from the thruster is smaller with the magnetic field. It was predictable regarding the thrust measurement, as explained before.

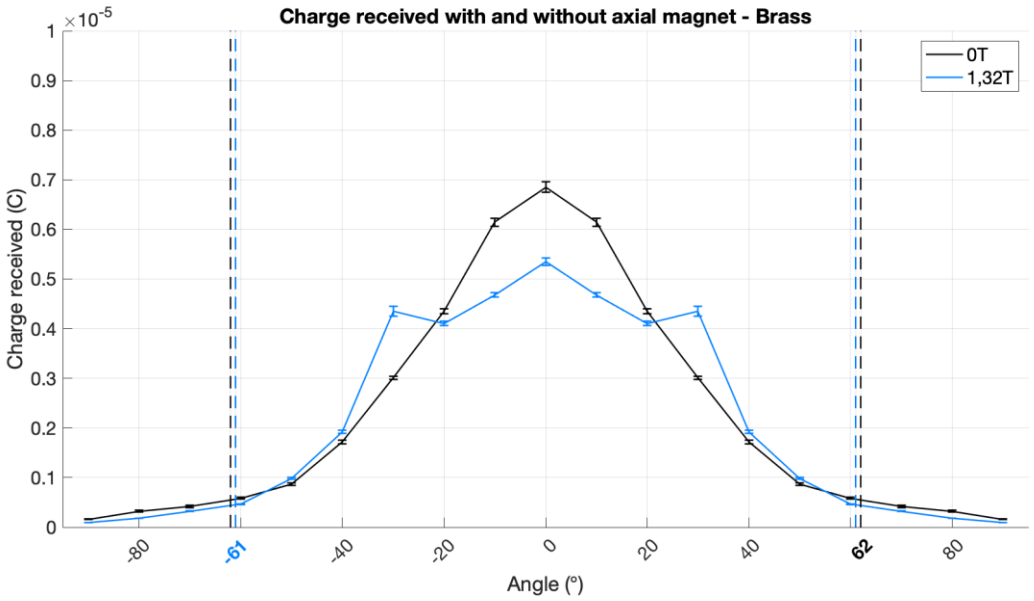

Figure 20. Cone angle for the brass cathode with and without the axial magnet (error bars represent the 95% confidence interval of all the *n* measurements)

About the titanium cathode, the cone angle is smaller with the magnetic nozzle, with 54° instead of 57°. As with the brass cathode, the spatial repartition of the charges shows a similar quantity of charges between 0° and 30° instead of a gaussian repartition seen without the magnet.

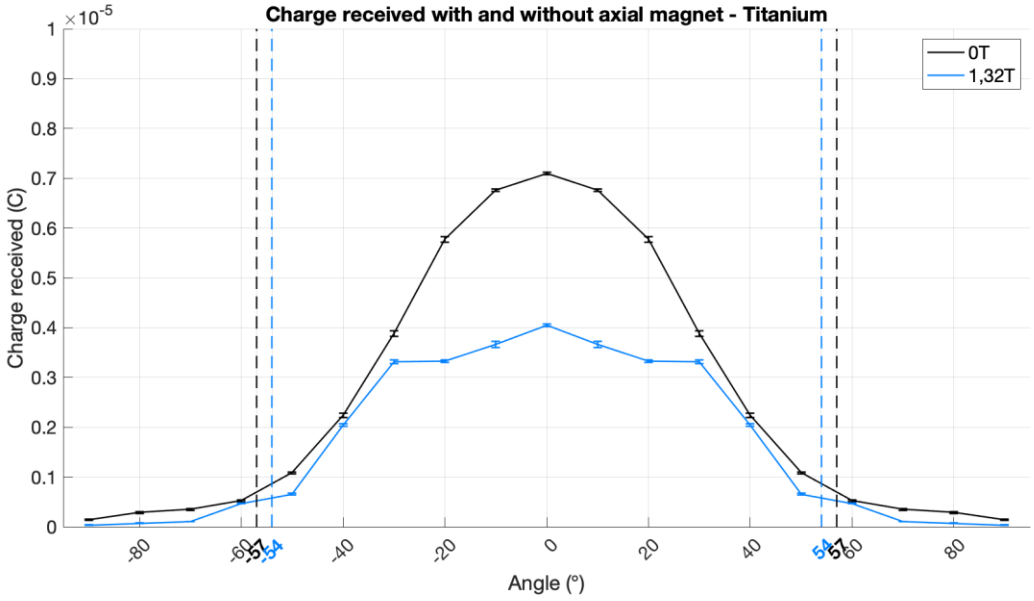

Figure 21. Cone angle for the titanium cathode with and without the axial magnet (error bars represent the 95% confidence interval of all the *n* measurements)

The main effect of the axial magnet seems to constrict the plasma plume by balancing the charge repartition between 0° and 30°. Consequently, the charge distribution is considerably modified and is no longer gaussian.

G. Mean charge state and mean velocity

The equations introduced in section III.A allow to determine the mean charge of the ions (Z) and their mean velocity ($\overline{v_i}$). The required parameters to find these values, the propellant mass eroded per pulse $m_{p/pulse}$, the ion current $I(\theta, t)$ and the impulse bit I_{bit}, were previously measured. Then, thanks to those results, the mean charge and the mean velocity arepresented is the following table:

Cathode material	Magnetic configuration	Z	$\overline{v_i}$ $(km.s^{-1})$
Brass	0T	1.16	30.6
	0.49T (radial)	1.32	33.3
	1.1T (radial)	1.23	29.9
	1.32T (axial)	1.07	24.0
Titanium	0T	1.99	31.5
	0.49T (radial)	2.05	31.9
	1.32T (axial)	1.37	32.4

Table 4. Mean ion charge state and mean ion velocity for each magnetic configuration and each cathode material

For the radially magnetized magnet, the mean ion velocity and the mean charge variations are correlated with the specific impulse. It means that these parameters increase between 0T and 0.49T and then decrease at 1.1T. Nonetheless, the axial magnet acts differently depending on the cathode material. On the brass cathode, it reduces both the mean charge and the mean velocity of the ions in the plasma flow, while on the mean velocity of the titanium ions is increased even if their mean charge is reduced.

H. Efficiency

The efficiency η of the PJP is given by the following equation, with E_d, the energy stored in the capacitor bank:

$$\eta = \frac{I_{bit} \cdot g_0 \cdot I_{sp}}{2E_d} \tag{19}$$

This value represents the ability of the thruster to convert electric energy into kinetic energy for the ions. The following figure presents the efficiency of the PJP depending on the different magnetic configurations.

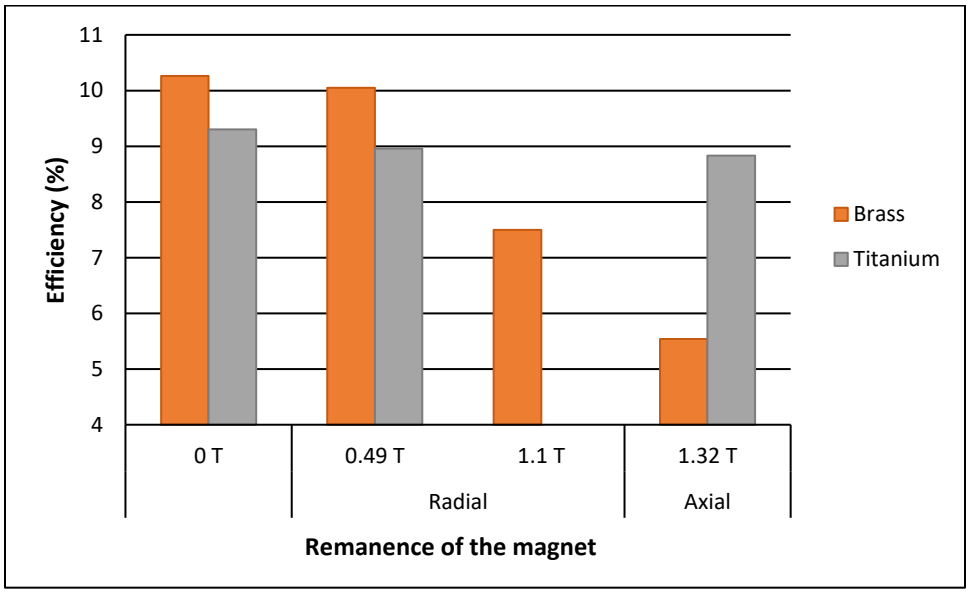

Figure 22. Efficiency of the thruster depending on the remanence of the magnet

The magnetic field reduces the efficiency of the thruster whether the magnet is radially or axially magnetized. Between 0T and 0.49T, the efficiency is similar, around 10% for brass and 9% for titanium. The radial magnet acts in the same way for both cathode materials. Conversely, the axial magnet has a different influence depending on the cathode material. The efficiency for the titanium cathode is lower than without magnetic by only 0.5%. For the brass cathode, the efficiency is almost divided by a factor 2 comparing to the non-magnetic configuration.

V. Discussions

The magnetic nozzles used in this study (radial and axial below 100mT on the anode vicinity) globally reduce the thruster efficiency. This study, added to the PJP heritage, highlights the difficulty to use a magnetic nozzle for such a VAT thruster. Even if the topology and the magnetic magnitude are the main parameters to drive the ion flux from the cathode region, it is tricky to find the best magnetic configuration with this kind of plasma characteristic (high density, short duration).

As presented in Figure 11, the impulse bit decreases for both materials with the radial magnets while in Figure 12 (axial magnet), the decrease is more important for the brass cathode compared to the titanium.

For the radially magnetized magnets, as it was presented from Figure 8 to Figure 10, the magnetic field at the center of the cathode is almost equal to zero. It is, actually, the area where the triggering arc discharge occurs and the cathode is heated. Consequently, we can assume that the influence of the magnetic field in this area is the same for both materials.

The axially magnetized magnet presents a high magnetic flux density at the center of the cathode. It means that all the plasma emitted between the ignition and the main discharge is within a non-null magnetic field. In this case, the magnetic field interacts with the cathode region, that is why we observed a major difference with the axial magnet on the performance.

It is notable that, for a given velocity and charge state, the area under the curve in Figure 15 tends to decrease as the remanence of the magnet increases. Consequently, the total charge exhausted from the thruster is smaller. It means that either the number of particles ejected is smaller or the mean charge of these particles is lower. In both cases, it is linked to the decrease of the efficiency.

The charge state seems to also have an impact on the curves presented in Figure 17 and Figure 18. Indeed, the most probable hypothesis is that the two peaks are signs of two ion populations. The first peak is represented by the most charged ions, on which the magnetic field has the most significant impact, but this population represents the smallest amount of the total ion flux. Conversely, the second population has a low mean charge (Z~2) and constitutes largely the ion flux. With the topologies and magnitude used in this study, the magnetic field is only able to focus and accelerates the first ion population.

VI. Conclusion

The intrinsic high speed characteristics of the PJP complicate the measurements of the physical parameters. Moreover, in order to have a low uncertainty on the specific impulse measurement, it is necessary to have a sufficient mass variation on the cathode. As the mass eroded per pulse is in the order of 1µg per pulse, a high number of pulses have to be performed to measure the mass variation on a precision balance with a resolution equal to 1mg.

Finally, the arc discharge occurring between the electrodes has a short duration (few tenths of µs) and a high current (2-5kA). These parameters make difficult the measurement of the ionic current in the plume (high frequency noise, filtering, etc.).

Two different magnetic topologies were used in this study, which create a permanent magnetic flux in the discharge chamber. The magnetic nozzles studied reduce both the impulse bit and the cathode mass consumed. Overall, the efficiency of the thruster decreases in all the magnetic configurations that have been tested for low magnetic field (below 100mT).

In the field of the Horizon 2020 program, a study of the PJP's magnetic nozzle has been realized by the Plasma Solve company[5]. The numerical simulation results highlight that the magnetic field must exceed a threshold of 100mT to obtain a significant effect on the ion flux.

The radial magnet tends to increase the ion kinetic energy but also the electron temperature which leads to a higher plume divergence. The electron pressure competes with the $j \times B$ term which lowers the divergence. Conversely, the axial magnet allows to significantly increase the thrust but only for very high magnetic flux density.

The main conclusion of this simulation is that the magnetic field has to be axially directed from the cathode to the anode in order to increase the efficiency. This magnetic configuration can only be achieved with an axial magnet or a coil. Using an axial magnet with a high magnetic remanence is tricky to implement in a satellite platform, as the magnetic momentum of the thruster has to be equal to zero. On the other hand, the coil option is difficult to implement on the PJP as the magnetic field generation has to be perfectly synchronized with the arc discharge and drastically increase the power consumption.

Finally, the impact of a magnetic nozzle on the PJP's performances is not straightforward. For magnetic fields below 100mT at the exhaust of the anode, the thrust efficiency tends to decrease. Regarding the numerical simulations, it appears that for magnetic fields higher than 100mT in the anode vicinity, the thrust efficiency can be increased and the plasma divergence can be reduced. Unfortunately, these best magnetic configurations are hardly applicable regarding satellite magnetic requirements (null magnetic moment, max magnetic flux density, etc.).
Further tests will be experienced and cross-checked by a dedicated numerical model on potential promising magnetic nozzle configurations. In parallel, a trade-off will be done to weigh the pros and cons of the magnetic nozzle implementation on the module.

Acknowledgments

Authors convey their thanks to the *European Union's Horizon 2020 research and innovation programme* under grant agreement No 870444.

References

[1] COMAT: https://comat.space/
[2] R. L. Boxman, D. M. Sanders, and P. J. Martin, "Handbook of Vacuum Arc Science and Technology: Fundamentals and Applications" Noyes Publications, 1995.
[3] E. Hantzsche, "A Simple Model of Diffuse Vacuum arc Plasmas," Contrib. Plasma Phys., vol. 30, no. 5, pp. 575–585, Jan. 1990.
[4] Blanchet, A., Herrero, L., Voisin, L., Pilloy, B. and Courteville, D. Plasma Jet Pack Technology for Nano-Microsatellites. In 36th International Electric Propulsion Conference, 2019.
[5] PLASMASOLVE: https://plasmasolve.com/